"Exploring Physiological Parameters in Dynamic WBAN Channels" , Max O. Munoz, Robert Foster and Yang Hao, IEEE Transactions on Antennas and Propagation, vol. 62, no. 10, pp. 5268-5281, 2014.

Exploring Physiological Parameters in Dynamic WBAN Channels

Max O. Munoz, Robert Foster, *Member, IEEE*, Yang Hao, *Fellow, IEEE*

Abstract— **On-body radio propagation in the 2.45 GHz ISM frequency band (2.40-2.48 GHz) was investigated during three different activities, jogging, rowing and cycling. Four different links were examined, from the waist to the wrist, ankle, chest and back; it was observed that the channel behavior could be related to the repetitive nature of the activities. Furthermore, combinations of the wrist, ankle and chest channels could potentially be used to identify the activity, whilst the waist-back channel show little variation between activities (roughly 2 dB, compared to 6-15 dB for the other links).**

The results also show that dynamic on-body radio channels contain rich biomechanical information, such as motion pattern, heartbeat and breathing process. It is demonstrated that physiological and kinetic features can, therefore, be extracted through some known signal processing techniques. For example, the repetitive nature of the activities introduces harmonics into the signal via the fading, which correspond to the speed of motion. In addition, the mechanical motion of the torso during respiration and cardiac activity also introduce harmonics due to changes in the path loss, albeit with low magnitudes. The detection of such signals is discussed.

Index Terms— **Wearable antenna, radio channel performance, electromagnetic wave propagation, on-body wireless sensors, physiological features.**

I. INTRODUCTION

THE continuous development of compact and low-power circuits has enabled the miniaturization of hardware systems and, thus, led to wireless pervasive sensing. The connection of different wireless nodes on and around the human body defines a Wireless Body Area Network (WBAN) [1, 2]. It is evident that particular areas of the body have unique characteristics, thereby affecting the performance of the radio channel [1]. Furthermore, external perturbations, such as human mobility [3] and operation in cluttered backgrounds [4], result in a complex environment for the propagation characteristics of body-worn sensors. Usually, these are comprised of low-power microcontrollers, tiny radio frequency (RF) transceivers and compact antennas that have low gain and narrow bandwidth (low-profile antennas).

Different studies have shown the potential use of wireless sensors during the healing process after surgery. Body-worn units housing accelerometers can monitor the level of activity

of a patient, indicating an improvement or a decline in recovery process (see, for example, [5, 6]). As a result, the quality of care provided to patients is improved by continuous monitoring, even those merely indicating general 'well-being'.

The transformation of future infrastructure (e.g., hospitals, military services and care centers) to support wireless sensing technology remains an essential and active part for future patient care. This will not only off-load demand for services, but will also promote autonomous and flexible monitoring solutions, especially for non-stationary scenarios, as patients need no longer be attached to large, stationary monitoring equipment while their vital signals are recorded. Taken together, these can reduce healthcare costs and improve daily lifestyles.

Many wireless systems have been proposed to accomplish this feat, with diverse solutions, ranging from wirelessly enabling existing medical devices to wireless non-invasive sensing of physiological parameters (e.g., [7, 8]). For example, in 1975, a non-invasive procedure to monitor respiratory movements was introduced by Lin; he later refined the technique to monitor the heartbeat [9-11]. The microwave system transmitted continuous wave signals from 2.1-2.5 GHz and the periodic displacement of the thoracic cavity was recorded in the reflected wave, which was phase-modulated by the time-varying position of the chest (a concept related to the Doppler Effect).

Further advances in technology made possible the design of compact and lightweight systems, improving not only the detection accuracy, but also reducing the phase-noise of the receiving signal. In [12], Doppler systems operating at different frequencies (i.e., 2.4 GHz, 5.8 GHz, 10 GHz, 26 GHz and 60 GHz, respectively) were considered. The results showed that the use of high frequencies (short wavelengths) vastly improved the sensitivity to small variations exhibited in chest-wall movements. Other studies made use of double-sideband transmission systems [13] and I/Q modulation (quadrature signals) [14], in order to reduce the number of the null points, a problem in single channel Doppler systems, and enhance the detection of cardiopulmonary movement. An alternative to Doppler-based sensing was proposed in [15], where motion-induced variation in the impedance of a planar resonator is combined with a SAW filter and an auto-regressive estimation technique to detect respiration and pulse rates.

The monitoring of human motion is frequently sensed by some combination of accelerometers, gyroscopes and inertial sensors, which are integrated with wireless modules (e.g.,

ZigBee, Bluetooth). In [16], a footwear-based activity monitor was implemented using accelerometers and pressure sensors to predict the energy expenditure associated with common daily postures and activities.

In [17, 18], the received signal strength (RSS), an internal parameter of RF transceivers, was used to characterize limb movements for kinesiotherapy activities using Crossbow IRIS wireless modules. Their results show that learning techniques, such as a Support Vector Machine, can determine and classify limb movements based on information from the fading in the propagation signal path.

Although most of these non-intrusive monitoring systems were studied and implemented in controlled environments using frequency domain techniques, signals recorded in time domain also embed external information.

On-body radio models, acquired from simulation and empirical methods, have shown that received signals are the combination of diffracted waves around the human body curvature, decaying creeping wave components and, to a high degree, scattered and reflected contributions (i.e., fast fading, multipath, shadowing) [19, 20].

Initial studies in [21] reported peak-to-peak signal variations of 16 dB between belt and shoulder-worn antennas when changes in body posture occurred. In [22], the walking process in different environments (i.e., anechoic chamber, open office area and hallway) was characterized. In the indoor scenarios, their results showed that the signal variations of different on-body channels were best described by a Nakagami-m distribution with a Level Crossing Rate (LCR) threshold of 20 dB below the median signal level.

The effect of polarization during motion was investigated in [23], with the consequent effect on fast fading also examined. It was found that motion affected the degree of shadowing observed and that polarization affected the mean path gain level.

A comprehensive examination of dynamic channels was given in [24], with a number of adult test subjects and with varying amounts of movement. Several statistical models were tested and ranked using Akaike's Information Criterion; of these, the Rayleigh model was consistently a poorer fit and the Weibull and Gamma distributions usually the best fits of those tested (though individual links could better fit other distributions, one of these two was usually a good approximation). Two alternative measurement campaigns were reported in [25]; the first, which did not distinguish between slow and fast fading, showed that the log-normal distribution was a good model in most cases and used the χ^2-test to determine goodness-of-fit. The second found that slow fading (shadowing) was best modeled with the Normal distribution, whilst fast fading was best modeled using either Rayleigh or Rice distributions. An RSS-based method was used in [26], to investigate the correlation of the shadowing characteristics of various on-body links. A moving-average filter was used to extract the shadowing components; correlation between channels was observed to be activity-specific.

Dynamic on-body propagation channels have also been examined in terms of the observed Doppler behavior whilst walking and jogging. For example, it was found in [27] that

there is a difference in amplitude in the Doppler response between polarizations (normal and tangential to the body surface) in the PSD. They found that using normal polarization antennas produced lower amplitudes of Doppler components than when using tangential polarization antennas, as channels with normal polarization are less affected by body scattering.

Asymmetric Doppler spectra are identified in [28] as resulting from off-body scatterers. The asymmetry resulted from the shadowing of the body of scatterers behind the body, as most of the on-body antennas were on the front of the body. The off-body contributions could mask the harmonics related to the body scatterers; however, the off-body scatterers were all at harmonics above 5 Hz. It is observed that the Doppler spectra again had harmonics around 1 Hz. This is also true of the results in [29]; in each paper, this harmonic is attributed to the motion of the body when walking or jogging. It is noted that there is an overlap of possible speeds in these activities, but that the mechanics of the motion differ, resulting in the observed differences between walking and jogging [29].

In this paper, custom-built wireless sensor nodes are used to evaluate the radio propagation characteristics of four on-body channels while different sport activities, selected for the periodic motion required, are executed. In addition, the collected radio propagation data are post-processed to investigate the ability to identify physiological markers, such as motion pattern, breathing process and heartbeat, from magnitude-only radio channel measurements, which are simpler and cheaper than those involving phase.

The rest of the paper is organized as follows: Section II describes the wireless sensor and the measurement procedure. In Section III, the received signal strength data recorded by the sensor node are analyzed for each on-body channel and exercise activity, to determine the channel fading characteristics in each case. It is assumed that the fading characteristics are strongly linked to the periodic motion of the body during exercise. Hence, in Section IV, the sensor node data are mapped to the frequency domain for analysis of motion and physiological signals, including a comparison with a normal electrocardiograph (ECG) signal. Further analysis is implemented using Fourier Transform models. Some conclusions are drawn in Section V.

II. MEASUREMENT PROCEDURE

Measurements were performed on a 168 cm tall, 80 kg male test subject. The transmitter node was fixed in the right waist section and the receiver node was in four different locations in succession: the upper middle section of the thoracic cavity (chest), the left ankle, the left wrist and the middle back (thoracic spinal cord). These locations were used for each physical activity. Fig. 1 shows the receiver and transmitter locations.

All the measurements were taken in Queen Mary's Human Performance Laboratory (indoor environment). The jogging exercise was performed on a motorized treadmill machine equipped with a digital display and an electronic console on the front panel. The tilt of the conveyor belt was set flat (no tilt), in order to simulate normal outdoor jogging.
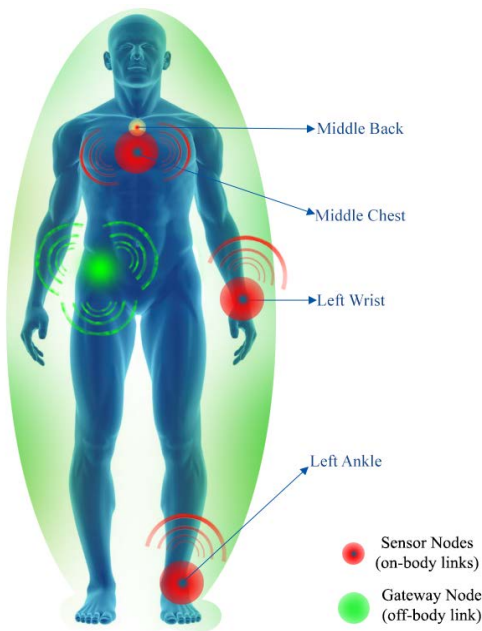
Fig. 1. Location of wireless sensors nodes (WSN) used in each athletic activity.

Cycling was carried out on a stationary professional training bike, where the resistance of the flywheel attached to the pedals was controlled by a digital control panel on the front of the bike. The test subject was seated with the body leaning forward and hands extended wide on the back part of the handlebar, simulating a normal outdoor pedaling. In the case of the rowing scenario, an air-resistance flywheel system, with a variable tension resistance control, was used. The rowing equipment was also fitted with a digital console control panel.

Each purpose-built wireless module is built around a Texas Instruments transceiver, the CC2420 [30], and an ultralow power microcontroller, the PIC18F2620 [31], which configures and controls the transceiver chip. The CC2420 is an IEEE 802.15.4-compliant transceiver [32] and was programmed to operate with a maximum output power of 0 dBm. In addition, it is specified to achieve a sensitivity level of -95 dBm (i.e., achieve a packet error rate of 1%, as required by the IEEE 802.15.4 standard [32]). The radiating element of each wireless sensor node was a microstrip patch antenna printed on top of a FR-4 substrate material of 1.6 mm thickness.

The system diagram of each wireless sensor node is shown in Fig. **2**a. The antennas for the nodes were designed and simulated using CST Microwave Studio [33], shown in Fig. **2**b, with the implemented antennas and the assembled low-power wireless module in Fig. **2**c. The normalized radiation patterns of the sensor node measured in an anechoic chamber are given in Fig. 3, when in free-space (not on the body) and when placed on the body. It is apparent that the free-space patterns show more backward radiation than the on-body results, as would be expected from the increased absorption by the body tissues. Good agreement between the patterns is seen for the right-half plane, for both polarizations. Differences are attributed to the body effect. A summary of the performance of the antenna and wireless sensor when on-body and free-space, together with the performance at different locations on the
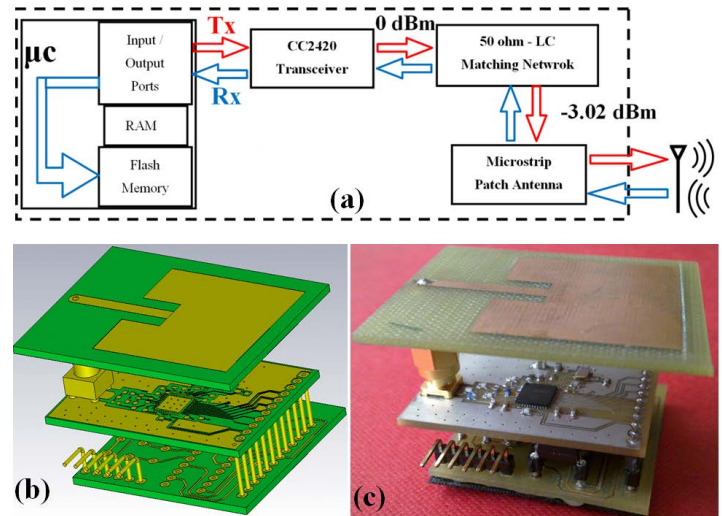

Fig. 2. Wireless module structure for used for on-body measurements and data logging: (a) internal block diagram of each low-power node [34]; (b) design structure implemented and simulated in CST Microwave Studio; (c) manufactured wireless sensor node.
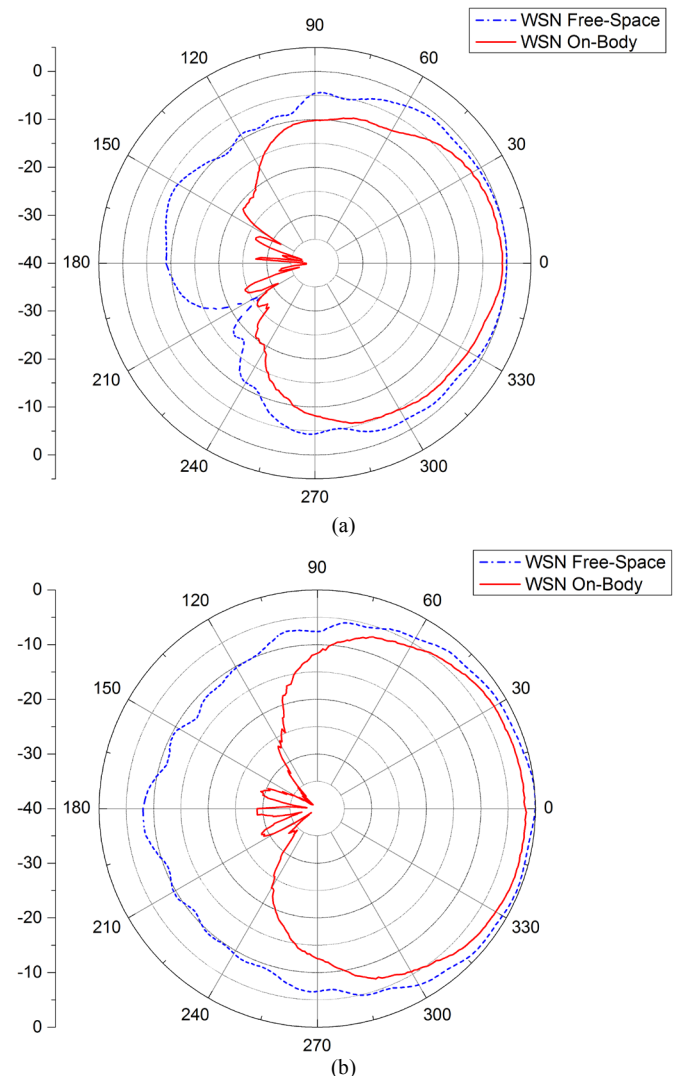

(a)

(b)

Fig. 3. Measured normalized radiation patterns of the wireless sensor nodes using horizontally polarized antennas when in free space and on-body (transmitter at waist level and receiver on chest section): (a) E-plane; (b) H-plane. Antenna pattern magnitudes are in decibels, angles in degrees.

torso, and the operation at different carrier frequencies (within the 2.45 GHz band), is described in [34].

For each activity, the receiver node recorded an average of 7000 samples of the RSS, at a rate of 14 ms per sample. In each activity, the receiver node began recording data only when the user reached a constant speed of 5 km/h, which was set and controlled by the digital control panel of each sporting machine. The acquired data were stored in the internal flash memory of the microcontroller and was later extracted for analysis.

In order to decrease uncertainties from location displacement due to the constant movement, VELCRO tape was fitted on the T-shirt and on the wireless sensors (i.e., transmitter and receivers). To confirm that the sensor data would not be corrupted by local movement of the node with respect to the mounting point, the effect of motion on the transmit antenna behavior was evaluated for the jogging activity. As the transmitter was located at the waist, local movement would be primarily reflected in a varying separation between node and body, changing the propagation environment for the antenna and, thus, its resonant frequency. Hence, monitoring the resonant frequency behavior serves as a proxy for monitoring local movement of the sensor node. In addition, this test was required to confirm that the variation was small with respect to the channel bandwidth (2 MHz, with a channel separation of 5 MHz, in IEEE 802.15.4 [32] [14]).

During the first two minutes, the subject was in a resting position (standing on the treadmill); for the next 10 minutes, the subject was moving (jogging at 5 km/h); and for the last minute, the subject was recovering (had stopped jogging). The performance of the transmit antenna (waist-location) for the aforementioned process is given in Fig. 4. Table I lists the main statistical parameters. It is apparent that there are small fluctuations in the resonant frequency of the antenna related to the repetitive motion, but these variations are small in magnitude, compared with the bandwidth of the antenna (less than 5% variation in standard deviation) or free-space resonant frequency (less than 0.3%, where f_0 is 2.45 GHz [34] [16]). Hence, local motion of the sensor nodes can be ignored. Furthermore, the maximum observed variation in resonant frequency was 2.6 MHz, implying that the use of a single channel (here, the sixth channel in the 2.45 GHz band) would not introduce significant uncertainties.

III. DATA ANALYSIS

A. Characterization of On-body Radio Channels for Dynamic Scenarios

It is evident that the practice of any sport activity will produce a high level of fluctuations on the received signal, which are the consequence of the continuous movement of the human body. In the case of jogging, our results show these variations are ±15 dB from the average received signal; this is significantly greater than received signals of a motionless user in a free-space environment, where the variations are ±3 dB.

The received signal for all scenarios considered (i.e., motionless, jogging, rowing and cycling) are shown in Fig. 5. The graphs plot a 45 s window length of a waist-chest channel.
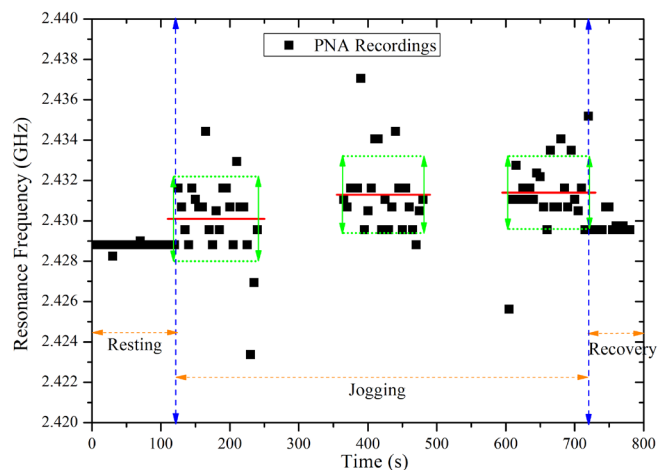

Fig. 4. Variation of the resonant frequency of the transmitting antenna for different stages (resting, jogging and recovery process).

TABLE I
VARIATION OF THE S_{11} RECORDED TO INVESTIGATE THE EFFECT OF LOCAL MOVEMENT AND CHANNELIZED MEASUREMENTS (F_0 − RESONANT FREQUENCY OF THE TRANSMIT ANTENNA IN FREE SPACE; S.D. − STANDARD DEVIATION; BW- TRANSMIT ANTENNA BANDWIDTH).

Process	Duration / min	Mean μ / GHz	μ/f₀ / %	S.D. σ / GHz	σ/BW / %
Resting	2	2.4288	0.16	0.00012	0.26
Jogging	2	2.4301	0.21	0.00210	4.42
Jogging	2	n/a	n/a	n/a	n/a
Jogging	2	2.4313	0.26	0.00190	4.00
Jogging	2	n/a	n/a	n/a	n/a
Jogging	2	2.4314	0.26	0.00180	3.79
Recovery	1	2.4298	0.20	0.00043	0.90

The mean values are −58.69 dBm, −54.6 dBm, −58.7 dBm and −62.81 dBm, respectively.

We use the difference between the known transmit power (-3.02 dBm) and RSS as a measure of the "power loss" of the channel, which includes the path loss and the gain of the two antennas. The statistics of the channel power loss (equivalently, of the RSS) can be described using probability density functions, discussed later in this section. The average power loss for each WBAN channel is described graphically as a function of box plots shown in Fig. 6. The spacing between the different parts of the box indicate the median and inter-quartile range; the length of the box and the position of the median with respect to the center of the box indicate the degree of dispersion (spread) and skewness of the logged RSS data, respectively. The mean is also indicated with a solid diamond marker. The mean power loss and standard deviation for each on-body channel are summarized in Table II. The results in Table II demonstrate that dynamic on-body channels present high variation amongst different links; however, the
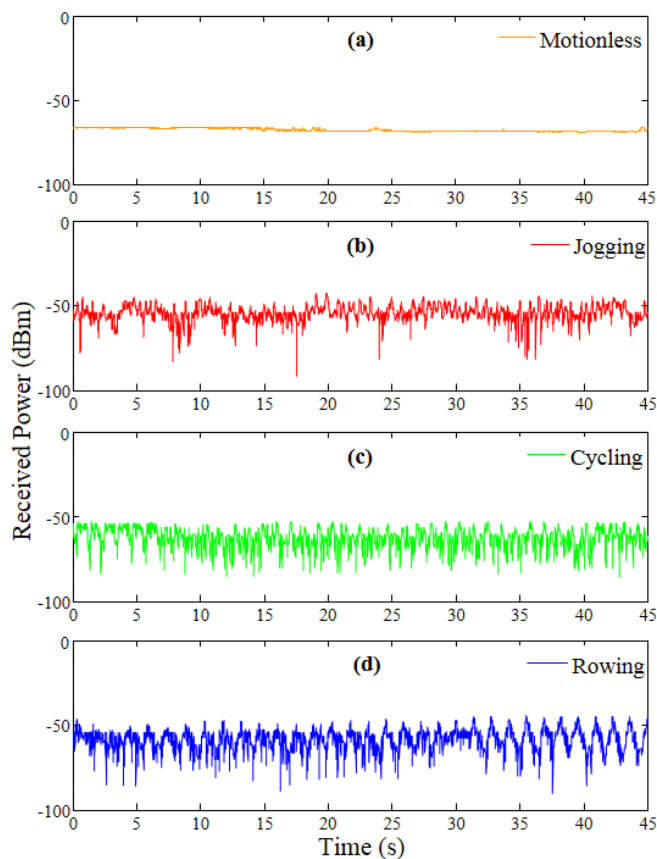
Fig. 5. Received signal for a waist-to-chest channel when the test subject is (a) motionless, (b) jogging, (c) cycling and (d) rowing.
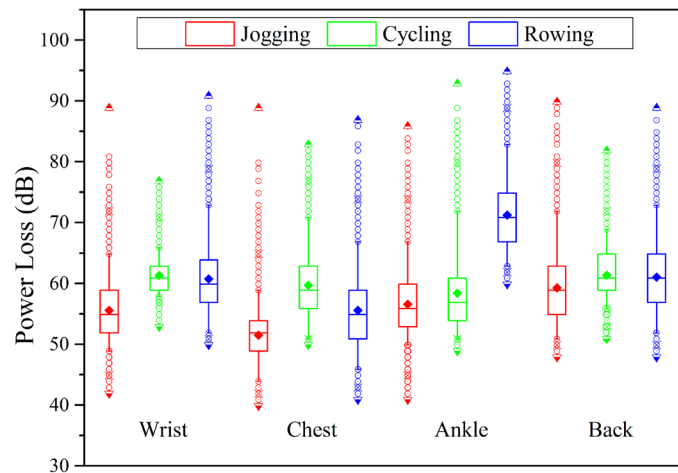

Fig. 6. Power loss at different on-body locations while the subject is undergoing a physical workout. ♦ - mean; ▲,▼ – extreme values; ○ – outliers.

back location presents the most correlated data between different actions. In the context of this study, *correlation* refers to a qualitative 'similarity of behavior' of a stated link between different activities, or to a qualitative 'similarity of behavior' of an activity between different links.

The observed correlation in the waist-to-back channel is consequence of the reduced movement, in contrast to other locations, particularly the wrist and ankle. Although the torso

TABLE II
STATISTICAL SUMMARY OF THE POWER LOSS VARIATION RECORDED BY CUSTOM-BUILT WIRELESS SENSOR NODES.

WBAN channel	Jogging		Cycling		Rowing	
Waist-to-	Mean μ / dB	S.D σ / dB	Mean μ / dB	S.D. σ / dB	Mean μ / dB	S.D. σ / dB
Wrist	55.55	5.14	61.27	2.82	60.74	6.16
Chest	51.45	4.99	59.66	5.95	55.55	6.32
Ankle	56.57	5.62	58.37	6.26	71.22	5.97
Back	59.23	6.46	61.31	4.37	61.05	6.23

may move significantly, the path length is essentially constant, as shown by the similar mean values for the different activities. Cycling shows a smaller degree of shadowing (as seen by the smaller standard deviation), as only the legs are moving, whereas both legs and arms are moving in the other activities.

The waist-wrist channel shows least variation (fading) during cycling; this is expected, as the arms are in a fixed position and fading only occurs through reflections from the moving legs.

The arms are also relatively far from the body, explaining the higher mean power loss. More variation is seen in the other two activities, because the arms are also moving, introducing more multipath components. The mean power loss is lowest for jogging, as the wrist spends a portion of each cycle relatively close to the waist. This is not true for rowing, where the wrist moves between the upper chest to being far from the body when the arms are fully extended, resulting in the higher mean power loss.

In the case of the waist–ankle channel, the jogging and cycling scenarios are highly correlated. This behavior is expected as a consequence of the constant speed of the user (5 km/h) and the nature of the motion involved in these activities, which is similar. On the other hand, the waist-ankle channel for the rowing scenario is uncorrelated with the jogging and cycling scenarios, which is the outcome of the constant action of leaning forward and backward. The motion of the ankle (and, to a lesser extent, the waist) is significantly different in this case.

The waist-chest channel demonstrates interesting behavior. The mean power loss is least in jogging and most in cycling. Jogging requires the body to be upright and with free space in front. For cycling, the torso is inclined forwards and is closer to the legs; there is thus always some part of one or both legs relatively close to the waist, changing the local environment and increasing loss. For rowing, at a given time instant, the legs and arms are totally extended and the torso is leaning back and extended; hence, path loss is higher, but loss in the body is relatively low. At a different part of the period, the knees and elbows are bent, bringing both legs and arms near the torso; hence, more loss occurs in the body. This would explain why the mean power loss during rowing is higher than in jogging,

but lower than in cycling. The variation in the standard deviation between activities is perhaps not as large; it is hypothesized that some of the variation comes from the different motion of the limbs in the different activities, but that some also comes from the motion of the torso itself. In particular, the torso moves most during rowing (extending and compressing) and least in jogging, which correlates with the observed behavior in standard deviation.

When comparing channels for a given activity, relatively wide variation in the mean power loss is observed for jogging and rowing, but not for cycling. It is believed that the mean path lengths for the four channels in the cycling activity are all roughly equal (for the test subject used), which is not true in the other activities. On the other hand, the standard deviations of the links vary most for cycling, not much for jogging and hardly at all for rowing. It is hypothesized that this reflects the nature of the shadowing from the body-motion for the different activities.

These results suggest that the combination of data from two or three channels would be sufficient to determine the respective activity. However, this requires further investigation.

Second-order statistics were examined for each measurement campaign. The measured received signal was normalized according to the maximum received power. The statistical analysis uses the square root of this normalized receive power in order to find normalized received signal amplitude.

The variation around the recorded received signal was modeled by six statistical distributions often used in WBAN communications (namely, the Lognormal, Nakagami, Gamma, Weibull, Rayleigh and Rician distributions) [1, 19-26]. All parameters were calculated on a 95% confidence interval according to their maximum-likelihood (ML) estimates. In addition, the Akaike's Information Criterion (AIC) score model was used to compare and evaluate the goodness of the fitting distribution for each sport activity. Because the sample size is finite, our study uses the second order AIC (AIC$_c$) model given by (2):

$$AICc = -2\ln\left(l(\hat{\theta}|data)\right) + 2K + \frac{2K(K+1)}{(n-K-1)} \quad (2)$$

where $\ln\left(l(\hat{\theta}|data)\right)$ is the value of the maximized log-likelihood over the unknown parameters (θ), given the data and the model, K is the number of parameters estimated for that distribution and n is the sample size.

The criterion was applied to evaluate the goodness of fit of the six commonly used distributions given above. A smaller value of AIC$_c$ means a better statistical model, and the criterion is used to classify the models from the best to the worse; to facilitate this process, the normalized AIC$_c$ (Δ_i) is considered and results are normalized to the lowest value obtained ($i = 1,…,6$, for the six distributions):

$$\Delta_i = AIC_{c,i} - \min\left(AIC_c\right) \quad (3)$$

A zero value indicates the model fits the data best of those compared. In this study, different sports activities are compared. In our analysis, we consider a time window of 45 s which states approximately 3215 samples ($n \approx 3215$), and all fitted distributions have a coefficient $K = 2$, except for Rayleigh, which has $K = 1$. The estimated distribution parameters, determined according to ML estimates, are presented in Tables III, IV and V for each sport application and link, together with the normalized AIC$_c$ values (Δ_i).

TABLE III
ML ESTIMATED DISTRIBUTION PARAMETERS FOR WBAN CHANNELS WHILE JOGGING AT A CONSTANT SPEED OF 5 KM/H

Jogging			Δ_i
Waist - Wrist	Lognormal	μ=-1.57, σ=0.59	2.10
	Nakagami	m=1.03, ω=0.074	2.00
	Gamma	a=3.47 , b=0.069	1.96
	Weibull	A=0.27 , B=1.96	2.00
	Rician	s=0.0078; σ=0.19	2.00
	Rayleigh	B=0.193	0.00
Waist - Chest	Lognormal	μ=-1.18, σ=0.61	2.42
	Nakagami	m=1.04, ω=0.16	2.00
	Gamma	a=3.31 , b=0.11	2.09
	Weibull	A=0.40 , B=2.1	2.00
	Rician	s=0.22; σ=0.24	1.99
	Rayleigh	B=0.28	0.00
Waist - Ankle	Lognormal	μ=-1.81 , σ=0.65	2.04
	Nakagami	m=0.89, ω=0.052	1.99
	Gamma	a=2.93 , b=0.067	1.93
	Weibull	A=0.22 , B=1.79	1.97
	Rician	S=0.0013; σ=0.16	2.00
	Rayleigh	B=0.16	0.00
Waist - Back	Lognormal	μ=-1.31 , σ=0.74	2.62
	Nakagami	m=0.79, ω=0.15	1.86
	Gamma	a=2.4 , b=0.14	1.96
	Weibull	A=0.38 , B=1.73	1.86
	Rician	S=0.001; σ=0.28	2.00
	Rayleigh	B=0.28	0.00

TABLE IV
ML ESTIMATED DISTRIBUTION PARAMETERS FOR WBAN CHANNELS WHILE CYCLING AT A CONSTANT SPEED OF 5 KM/H

Cycling			Δ_i
Waist - Wrist	Lognormal	μ=-0.97, σ=0.32	1.37
	Nakagami	m=3.07, ω=0.17	1.15
	Gamma	a=10.81, b=0.037	1.22
	Weibull	A=0.44, B=3.86	1.13
	Rician	S=0.38; σ=0.11	1.12
	Rayleigh	B=0.29	0.00
Waist - Chest	Lognormal	μ=-1.13, σ=0.68	2.83
	Nakagami	m=0.85, ω=0.21	1.88
	Gamma	a=2.67, b=0.15	1.92
	Weibull	A=0.44, B=1.79	1.86
	Rician	S=0.012; σ=0.32	2.00
	Rayleigh	B=0.32	0.00
Waist - Ankle	Lognormal	μ=-1.09, σ=0.72	9.14
	Nakagami	m=0.95, ω=0.20	1.99
	Gamma	a=2.78, b=0.14	2.64
	Weibull	A=0.45, B=2	2.00
	Rician	S=0.28; σ=0.25	1.96
	Rayleigh	B=0.32	0.00
Waist - Back	Lognormal	μ=-1.20, σ=0.50	1.96
	Nakagami	m=1.29, ω=0.14	1.92
	Gamma	a=4.45, b=0.076	1.87
	Weibull	A=0.38, B=2.22	1.96
	Rician	S=0.00072; σ=0.26	2.00
	Rayleigh	B=0.26	0.00

TABLE V
ML ESTIMATED DISTRIBUTION PARAMETERS FOR WBAN CHANNELS WHILE
ROWING AT A CONSTANT SPEED OF 5 KM/H

Rowing			Δ_i
Waist - Wrist	Lognormal	μ=-1.25, σ=0.71	2.33
	Nakagami	m=0.80, ω=0.17	1.85
	Gamma	a=2.51, b=0.14	1.83
	Weibull	A=0.4, B=1.72	1.82
	Rician	S=0.012; σ=0.29	2.00
	Rayleigh	B=0.29	0.00
Waist - Chest	Lognormal	μ=-1.69, σ=0.73	1.83
	Nakagami	m=0.71, ω=0.079	1.85
	Gamma	a=2.31, b=0.1	1.73
	Weibull	A=0.26, B=1.57	1.79
	Rician	S=0.0064; σ=0.2	2.00
	Rayleigh	B=0.2	0.00
Waist - Ankle	Lognormal	μ=-1.31, σ=0.69	2.42
	Nakagami	m=0.87, ω=0.14	1.96
	Gamma	a=2.69, b=0.12	2.03
	Weibull	A=0.37, B=1.82	1.96
	Rician	S=0.0005; σ=0.27	2.00
	Rayleigh	B=0.27	0.00
Waist - Back	Lognormal	μ=-1.52, σ=0.72	1.92
	Nakagami	m=0.75, ω=0.11	1.86
	Gamma	a=2.38, b=0.11	1.77
	Weibull	A=0.31, B=1.63	1.82
	Rician	S=0.005; σ=0.23	2.00
	Rayleigh	B=0.23	0.00

Fig. 7. Probability Distribution Function (PDF) for a waist-to-back channel recorded by custom-built wireless sensor nodes operating at 2.45 GHz while the test subject was jogging at a constant speed of 5 km/h.

Fig. 8. Probability Distribution Function (PFD) for a waist-to-ankle channel recorded by custom-built wireless sensor nodes operating at 2.45 GHz while the test subject was rowing at a constant speed of 5 km/h.

The lognormal distribution has been commonly applied to describe static and off-body WBAN communication channels (e.g., [1, 35, 36]). In our study, however, it was observed that Rayleigh distribution is consistently the best fit to the measured data, according to the AIC_c scores, followed by Nakagami and Weibull distributions; these three are commonly used to model strong fast fading, suggesting that the observed channel dynamics are dominated by fast fading. We did not attempt to evaluate an overall "best" model for all links and activities, as our primary aim in this analysis was to provide some insight into the channel behavior for each combination of link and activity. However, it is apparent that the Rayleigh distribution would fulfil this role, for our data. It would be interesting to determine whether this remains true when varying the test conditions (e.g., speed of activity, subject, activity, test environment).

Plots of probability distribution functions (PDF) as functions of the normalized instantaneous received power are shown in Fig. 7 and Fig. 8. The bin size of the histograms used to describe the PDF of the measured data is chosen according to the "Freedman-Diaconis" rule [37, 38].

IV. EXPLORING ON-BODY RADIO CHANNELS FOR EMBEDDED PHYSIOLOGICAL FEATURES

The previous section identified statistical distribution models that describe the behavior of dynamic on-body radio channels. It also showed that received signals are highly variable due to the constant change of frequency, amplitude and phase with time. Although there is a high amplitude variance in the received signals, the use of wireless sensors certainly represents a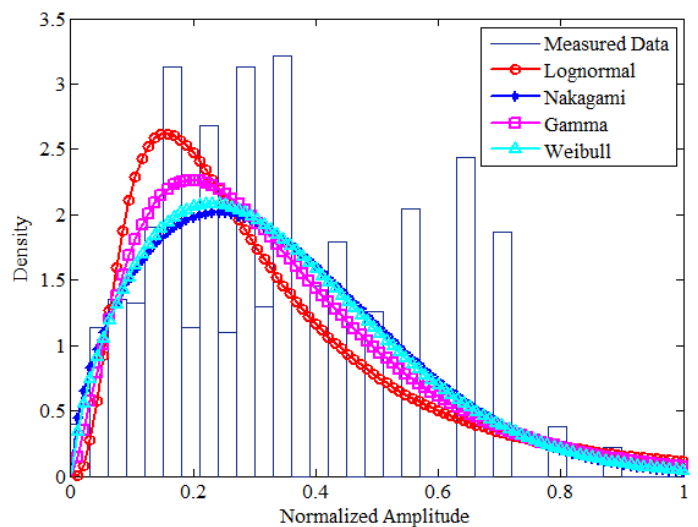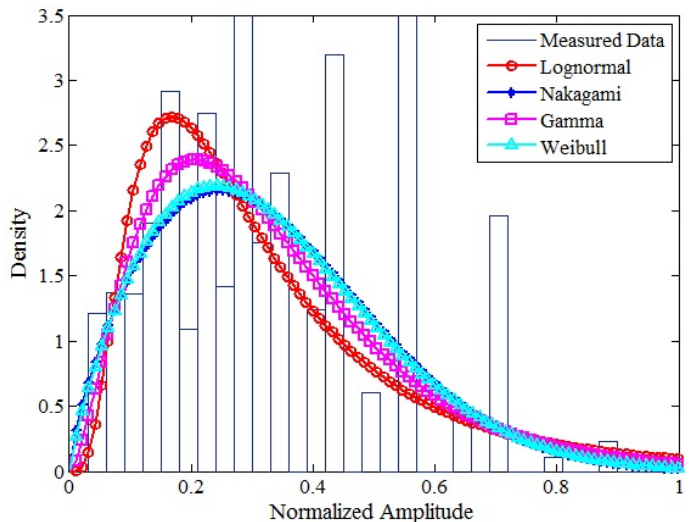 flexible and sustainable solution for environments where freedom of movement is needed. In this context, the current section explores the on-body electromagnetic (EM) wave propagation, recorded by wireless sensor nodes, as a sensing method. Specifically, we seek to analyze the fading behavior, characterized in Section III, to see how the motion of the test subject affects it. In order to maximize the identification and extraction of physiological features, such as respiration rate or heartbeat, the study only considers waist-to-chest channels; any effect on the other channels would be smaller in magnitude.

The use of powerful and robust digital signal processing techniques (e.g., template matching, blind source separation, or wavelet transforms) is undoubtedly advantageous; however, the latter is beyond the current study, and hence a combination of digital filtering and spectral response is presented.

A. Physiological Information Parameters

The number of breaths and heartbeats per minute varies with the subject's body mass index (i.e., the ratio of body's weight and the square of height), age, gender and, of course, the activity level. The pulse rate of a resting adult has an average frequency of 1-1.5 Hz, or 60 to 90 beats per minute (BPM). On the other hand, the resting respiration rate is about 6-12 breaths/min [10, 39]. The mechanical processes of the cardiovascular and the respiration cycles produce abdominal displacements of 0.2-0.5 mm and 4-12 mm, respectively.

During a normal walk, the pulse increases up to 95 BPM and the respiration rate varies between 12-18 breaths/min, while performing other athletic activities (such as running, swimming, rowing or cycling) causes the heartbeat rate to increase to almost twice that of a resting adult: 120 to 190 BPM (2-3.1 Hz, respectively) [39].

Considering an average heartbeat frequency of 2.6 Hz ($f_{heartbeat} = 2.6$ Hz) for a workout activity of an adult, the minimum sampling frequency, defined by Nyquist-Shannon theorem, should be 5.2 Hz (i.e., $t_s = 192$ ms), in order to perfectly reconstruct the original signal. The average sampling rate of the custom-built wireless sensors is 14 ms/sample (71.4 Hz), a high margin from the minimum sampling rate.

The data acquisition for the jogging scenario was executed on a computerized Cortex system controlled by a software application called MetaSoft Studio [40]. The application software manages and monitors both ECG recordings and jogging speed (5 km/h).

The integrated system, shown in Fig. 9, was not used for cycling and rowing activities because the large number of cables across the body was restricting the normal workout process.

The ECG recording device was a certified 12-Lead electrocardiograph, the Cardio-Collect 12. The sampling frequency and the ADC resolution of the system were 500 Hz and 12 bits, respectively. The cardiac recordings were taken for both the resting position (standing on the treadmill machine) and jogging (constant speed of 5 km/h), while the wireless sensor nodes recorded RSS values only when a constant speed was achieved.

The acquired ECG waveform, which served as a reference waveform for the cycling and rowing scenarios, showed a normal sinus rhythm without any significant arrhythmias. A 10 s sample frame for resting and jogging scenarios is shown in Fig. 10. In addition, heart rate variability during a five-minute period is described in Table VI.

B. Frequency Analysis of Time-Domain Channel Data

The spectral estimation was performed for four different scenarios: resting (0 km/h), jogging, cycling and rowing (each at 5 km/h). Normalized received signals were filtered using a tenth-order elliptic band-pass infinite impulse response filter. A finite impulse response filter was not used because the received data does not contain any phase information; hence, phase linearity was not necessary. The digital filter was computed on data segments of 45 seconds (≈ 3215 samples).
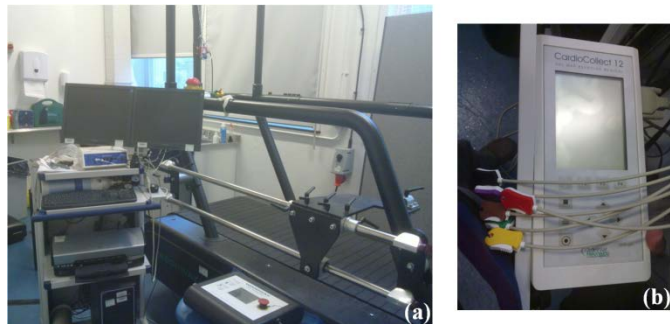

Fig. 9. Queen Mary's Human Performance Laboratory: (a) integrated Cortex System synchronized with a treadmill machine and electrocardiograph; (b) 12-Lead electrocardiograph system Cardio-Collect 12.
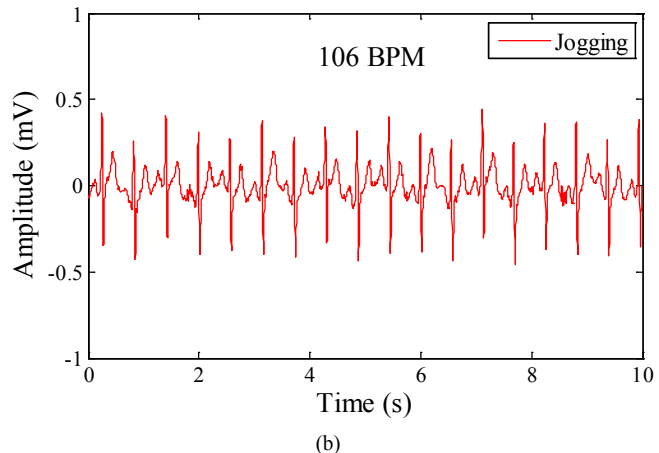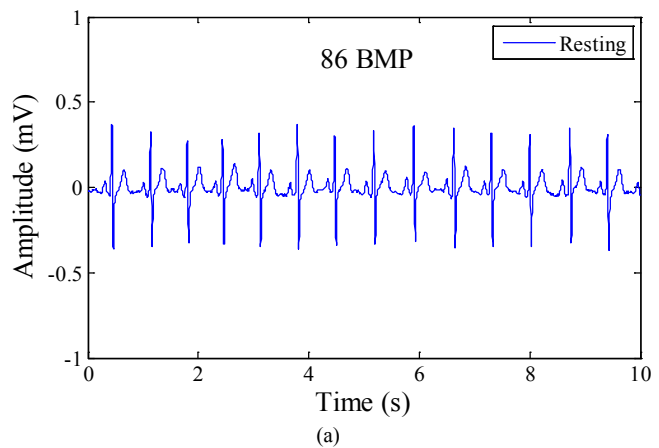

(a)

(b)

Fig. 10. Heartbeat signal of the test subject while is: (a) standing on the treadmill machine (resting stage). The average heartbeat was 86 BPM; (b) jogging at a constant speed of 5 km/h. The heartbeat rate was 106 BPM.

TABLE VI
HEART RATE (H.R.) VARIABILITY FOR A RESTING AND JOGGING SCENARIOS
CALCULATED FROM A 5 MINUTE SEGMENT FRAME

Scenario	H.R. Mean / BPM	H.R. S.D. (σ) / BPM
Resting	86.07	4.83
Jogging at 5 km/h	106.3	4.29

In order to avoid frequency component confusion when evaluating the signals for respiration rate and heart rate, two different band-pass filters were implemented: the first filter with cut-off frequencies of 0.1 Hz (lower frequency) and 0.8 Hz (higher frequency) for breathing analysis and the second filter with cut-off frequencies of 0.8 Hz (lower frequency) and 3 Hz (higher frequency) for heartbeat and movement analysis. This was based on the expected range of values for these sources.

The frequency domain analysis was based on the estimation of the power spectrum density (PSD) from filtered data. The PSD evaluation methods can be divided into parametric (e.g., autoregressive modeling) and non-parametric (e.g., Welch's periodogram [41]) methods. The non-parametric methods are, in general, faster to compute and, in the case of Welch's FFT method, it reduces the variance of the spectral density by averaging. This method divides the time series samples into overlapping sub-sequences. Each sub-sequence is windowed and then the estimated spectral density is averaged (our study uses a Hann window).

The Hann window [42] is used to smooth uncorrelated data located at the edges, diminishing aliasing of different rooted information and minimizing the amplitude dispersion into other harmonics (i.e., reduced spectral leakage). Additionally, the window function limits the extent of the sequence, providing a more stationary spectral characteristic.

The Hann window function is given by:

$$w_n = 0.5\left(1 - cos\left(2\pi \frac{n}{N}\right)\right) \quad for \quad 0 \le n \le N \qquad (4)$$

The terms n and N in (4) represent the discrete-time index and the length of the window, respectively. The window length was selected such that reasonable spectral performance was achieved. In the analysis, N was limited to 4096 samples (without zero padding) with window sections of 1024 and window overlaps of 512.

The spectral content of a resting scenario (test subject standing on the treadmill machine) was taken for five different locations along the upper chest section. The resulting plot, shown in Fig. 11, depicts the main component at these locations, which occurs between 0.12 Hz and 0.13 Hz; assuming that this is a result of the movement of the chest due to respiration, this would be equivalent to a breathing rate of 7.2-7.8 breaths/min. The spectral results of the second filter (0.8-3 Hz) did not show any significant harmonics to be related with heart beat movement; therefore, it was not included.

The difference between the curves is attributed to the change in path loss associated with the change in receiver location. Recall that the transmitter is fixed at the right waist.

Position 1 is on the furthest right part of the chest and has the shortest path length, which increases to its maximum at position 5. Hence, path loss is lowest at position 1 and highest at position 2, reflected in the amplitude variation. The small variation in the location of the main harmonic is attributed to small movements by the test subject.
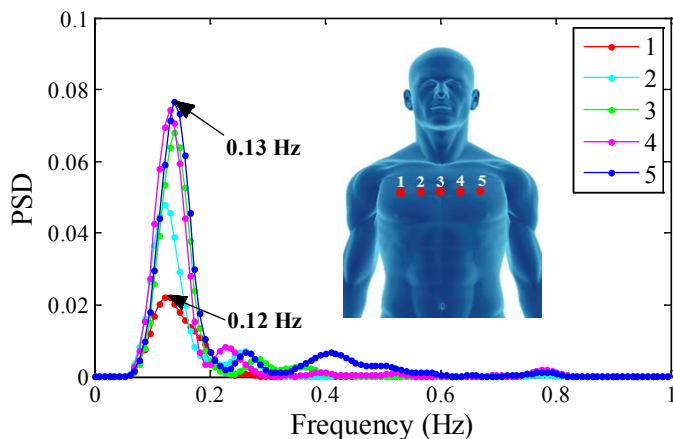

Fig. 11. Power spectral response recorded by WSNs for five different positions alongside the trunk section while the test subject is resting (standing on the treadmill machine). PSD values are absolute amplitudes in milliwatts.

The filtering method was also applied to each RSS signal recorded while jogging, rowing and cycling. The spectral responses of the implemented digital filters are illustrated in Fig. 12. The results of the jogging scenario (see Fig.12a) show a sub-harmonic at 0.14 Hz (lower frequencies), which could be regarded as the thoracic displacement produced by the breathing process (approximately 8.5 breaths/min). At higher frequencies, two main harmonics are clearly visible, the first at 0.9 Hz and the second at 1.8 Hz. It is known that human locomotion depends on two main factors, stride length and stride frequency, both of which contribute to a jogging activity. The constant speed of 1.38 m/s and the average stride length of 1.5 m give rise to the first harmonic, 0.9 Hz. This is the fundamental component product of the periodic kinematic of the human body, which is mainly dominated by the head and the thoracic cavity.

The 1.8 Hz harmonic, which is twice the fundamental frequency (0.9 Hz), could also be described by the quasi-synchronous movement of the arms and legs. If we examine the sequence (a)-(b)-(c), depicted in Fig. 13, the left-arm and the right-leg go up-front during the initial step succeeded by the right-arm and the left-leg, shown in sequence (d)-(e)-(f), for the following step. The cyclic movement of the extremities, which is repeated during the entire jogging process, shadows the propagation channel, and thus produces a harmonic at 1.8 Hz.

As mentioned in Section I, others have investigated the Doppler behavior of dynamic WBAN channels when walking and jogging (for example, [27-29]). It is important to note that this study does not measure the phase of the received signal and is thus not able to assess the Doppler spectra; we are interested in whether the fading characteristics allow activity-related parameters to be determined from magnitude-only measurements, which are simpler and cheaper to perform. However, it is possible to make some comments and comparisons with such work.

As mentioned previously, it was found in [27] that using normal polarization antennas produced lower amplitudes in the

Doppler response than when using tangential polarization antennas, as channels with normal polarization are less affected by body scattering. Typical normalized amplitudes of harmonics around 1 Hz are −30 dB for normal polarization channels [27], which compares well with the results in Figs. 11 and 12(a). We note that the patch antennas used in our study are horizontally polarized and radiates normal to the body.

Off-body scatterers in complex environments were observed to affect Doppler spectra in [28]. The off-body contributions could mask the harmonics related to the body scatterers; however, the off-body scatterers were all at harmonics above
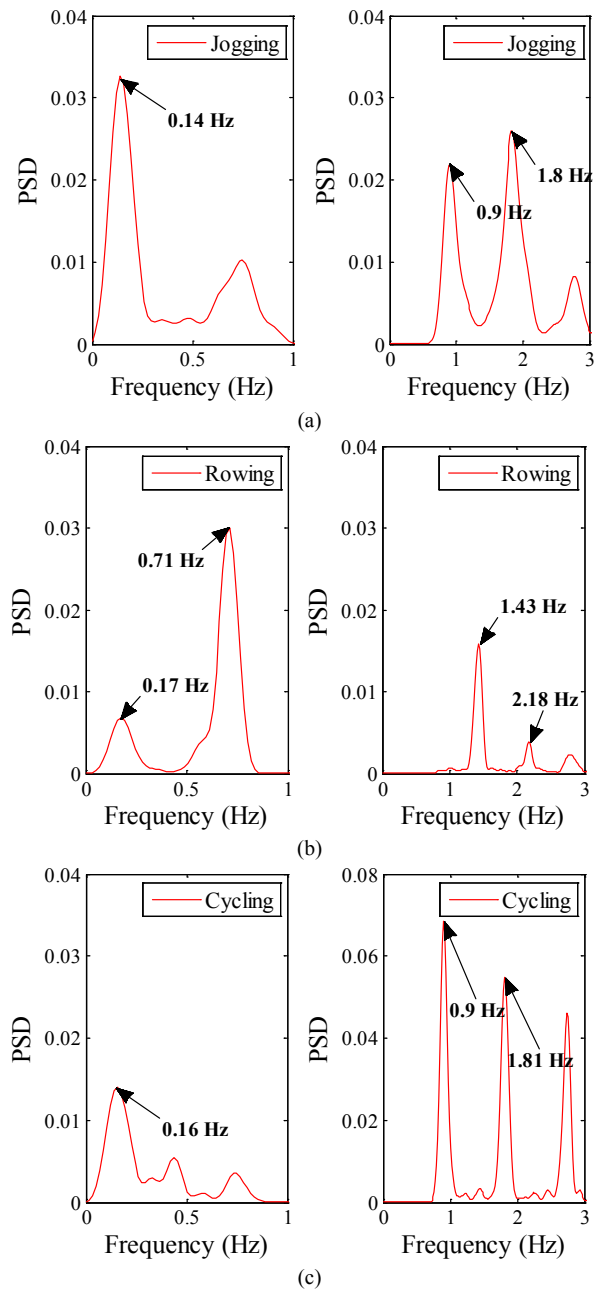
5 Hz, and so should not affect the results we observed. It is noted that the Doppler spectra again had harmonics around 1 Hz. This is also true of the results in [29]; in each paper, this harmonic is attributed to the motion of the body when walking or jogging. We note that there is an overlap of possible speeds in these activities, but that the mechanics of the motion differ, resulting in the observed differences between walking and jogging [29].

We also note that the Doppler spectra in [27-29] are centered at 0 Hz. This seems reasonable, as both the moving nodes and the body scatterers are likely to move towards and away from the receiving node during the course of walking or jogging. This result cannot be verified from our data, unfortunately; as we are dealing with a magnitude-only measurement, a two-sided spectrum would be a mathematical construction that would necessarily be centered on 0 Hz. Furthermore, we are dealing with filtered (band-limited) data.

The frequency domain plot for the rowing activity has two main components at lower frequencies (namely, 0.17 Hz and

Fig. 12. Power spectral density response using Welch's method for RSS signals while the test subject is (a) jogging; (b) rowing and (c) cycling. All the activities are performed at a constant speed of 5 km/h. The left hand plots use data pre-filtered using a BPF between 0.1-0.8 Hz; the right hand plots use data pre-filtered using a BPF between 0.8-3.0 Hz. PSD values are absolute amplitudes in milliwatts.
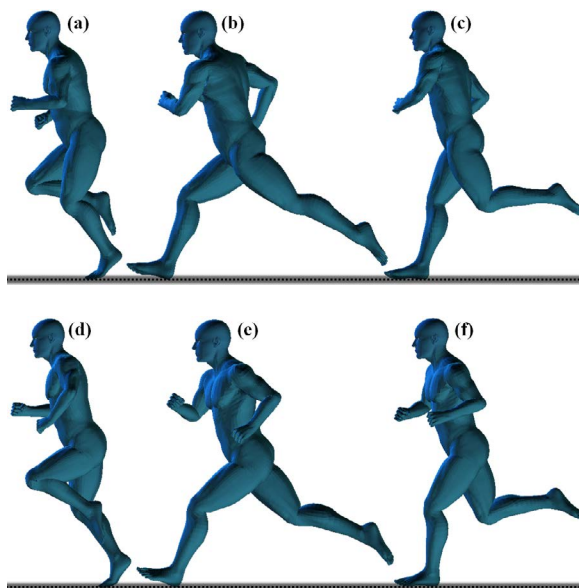

Fig. 13. Snapshot sequence of the human body movement during a jogging exercise, modeled in POSER: (a), (b), (c) represent the initial forward step and (d), (e), (f) correspond to the next forward pace.
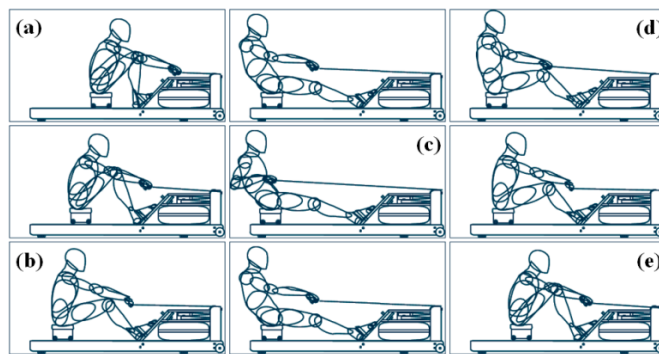

Fig. 14. A common sequence during a rowing process: (a) the catch, (b) the drive, (c) the finish, (d) the recovery and (e) the return to catch.

0.71 Hz) and two higher harmonics, at 1.43 Hz and 2.18 Hz, respectively (see Fig. 132b).In order to explain the source of each harmonic, it is necessary to unfold the steps of a rowing process. A normal rowing technique is divided into four main phases: the initial part of a stroke, where the body is pressed up to the legs and shins are vertical, thus preparing for the next pull, is regarded as *the catch* (shown in Fig. 14a). The following phase, called *the drive* (Fig. 14b), is initiated when the body's main hip extensors (legs and glutes) push down as the body levers back but the arms remain straight (transfer of power stage). The next state, where the legs are fully extended and flat, and the rowing handle is located at the abdomen position, is defined as *the finish* position (Fig. 14c). The final part of a stroke, called *the recovery* process (Fig. 14d), is a slow slide back to the initial position (actions are in reverse order compared with the drive phase), thus returning to the catch position (Fig. 14e).

The component at 0.17 Hz is mainly attributed to the thoracic movement produced by the breathing process, which would correspond to an average respiration rate of 10.2 breaths/min. During the rowing process, the test subject worked out at a constant speed of 5 km/h, covering an average distance of 1.8 m for each stroke (catch-finish, finish-catch).

The continuous levering backward and forward of the body, from *catch* to *finish* position, produces the fundamental component of 0.71 Hz. Similar to the jogging scenario, the 1.43 Hz tone is close to the second harmonic of the fundamental frequency; a close examination of the rowing process also shows that, amid each stroke, the rowing handle crosses the transmitter node twice (i.e., shadowing the free-space propagation). The first instance is when the body lays back to *the finish* stage and the second time is when *the recovery* phase takes place, thus producing a 1.43 Hz component.

The last spectrum plot corresponds to the cycling scenario (see Fig. 12c), where the main components are observed at 0.16 Hz for the lower frequencies, and 0.9 Hz and 1.81 Hz for the higher frequencies. The cycling process is mainly dominated by the pedaling sequence. Key snapshots of this routine are shown in Fig. 15a-c. The movement created by the rotation of the legs around the circumference of the pedal crank is defined by the sprocket-arm (length = 0.20 m) and the bike ergometer's speed (5 km/h). The angular movement of the right leg brings about periodic displacements of the transmitter node, which is located on the same side but at waist level, thus defining a cyclic translation of approximately 1.06 Hz and hence an angular speed of 64 rpm. In addition, the link (Tx – Rx) is shadowed twice per cycle, or every π radians, thus defining a frequency of 1.81 Hz.

The motion observed during cycling is mainly dominated by the leg movement, whereas the chest area remains fairly motionless (i.e., leaning forward towards the handlebar with relaxed arms; see Fig. 15a-c), in contrast to the other activities. This type of body posture creates a cavity section for the EM propagation, which maximizes the number of waves travelling along the body; hence, the 0.16 Hz harmonic is interpreted as a result of the respiration process, which would be equivalent to 9.6 breaths/min.
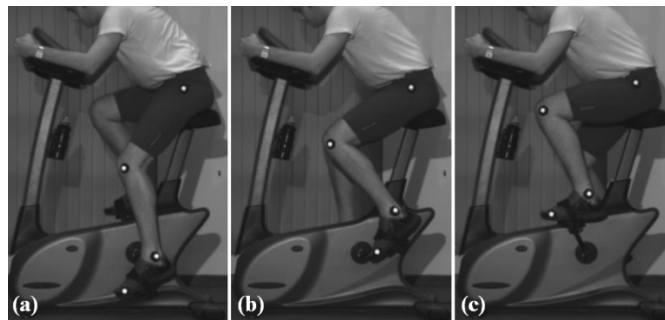

Fig. 15. Cycling at a constant speed of 5 km/h, (a)-(c) Snapshots of main movements of the human body while (Images are for illustration purposes only) and (d) normalized spectrum response of the received signal.

It is evident that the spectral content is mostly accounted for by the motion of the body and its parts, with some potentially contributed by the respiration process. This is unsurprising, when considering the relative magnitudes of the displacements involved, and of the resulting shadowing effects. However, to determine how the heart beat motion might contribute, the spectral response of the recorded ECG signals (for the resting and jogging scenarios, see Fig. 10) was calculated to predict where the expected harmonics would occur; the results are shown in Fig. 16a-b. In both cases, the noise introduced by the mains was removed using a digital notch filter operating at 50 Hz to 60 Hz.

The resulting plots show a main harmonic at 1.46 Hz (for a resting scenario), equivalent to a heart rate of 87.6 BPM. In contrast, the jogging scenario ECG has two main frequency components: the first at 1.04 Hz and the second at 1.71 Hz. The former is possibly caused by electrode movement due to the constant human motion; however, this requires further investigation. The latter is the cardiac signal (being equivalent to a heart rate of 102.6 BPM), based on a comparison with the recorded ECG signal.

It is noted that the transformation from time to frequency domain has introduced a HR deviation of 1.77% and 3.4%, for resting and jogging scenarios, respectively. This deviation is mainly attributed to the FFT coefficient rounding errors and floating point arithmetic quantization errors.

A summary of the spectral content of each scenario is presented in Table VII. The table includes sub-harmonics and main frequencies for each recorded activity, including the spectral components of the electrocardiograph. It can be seen that the second harmonics of jogging and cycling are similar to the main harmonics of the ECG; however, this is likely a coincidence, given the analysis presented above. A more rigorous study is required considering additional important aspects, such as different speeds and stride lengths. Furthermore, a more sensitive setup, possibly at higher frequencies, may be necessary before the shadowing from the motion of the chest due to the heartbeat can be detected.

Our results have shown that the respiration rate could potentially be estimated from the shadowing caused by the thoracic movement produced over a period of time (see Table VII), but that the heartbeat rate is not evident. This due to the scale of motion induced, and the correspondingly small fluctuations in path loss expected, by the heart when beating.
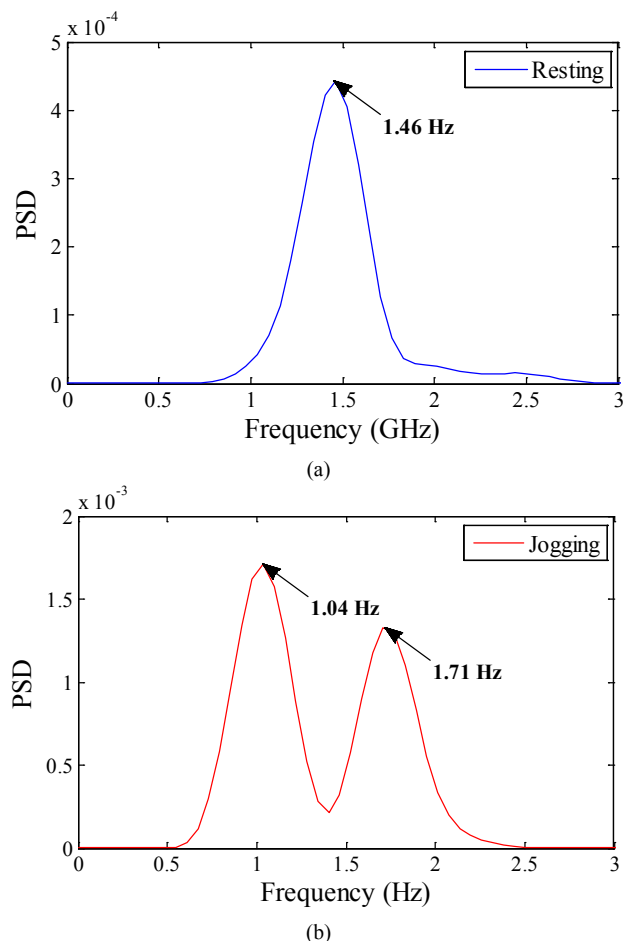
(a)

(b)

Fig. 16. Power spectral density response using Welch's method for recorded ECG signals while the test subject is: (a) standing on the treadmill machine (resting stage); (b) jogging at a constant speed of 5 km/h.

This was confirmed by the use of an ECG to identify where the harmonics should be (possible as the ECG records the electrical variation of the heart over a period of time across the electrodes, whereas the wireless sensor nodes detect the mechanical movement). However, the spectral analysis has shown that features related to the specific activity are easily identifiable. This may have applications in sports training and physiotherapy. We note that the relative movement of the thorax becomes more significant as the frequency of the propagating EM wave increases, suggesting a higher frequency would be more sensitive to respiration and even possibly heart activity. However, there would be an upper limit to the useful frequency for a given transmit power, due to increased losses. Finding the optimum point is an objective for future work.

V. CONCLUSIONS

The paper presented the radio-channel characterization of different on-body links for assorted body movements. It was first shown that the continuous movement of the human body, trunk and the limbs, for non-stationary scenarios (e.g., jogging exercise) shadows the line-of-sight propagation, thus producing signal fluctuations of ±15 dB (maximum level from the average received signal).

TABLE VII

SUMMARY OF MAIN HARMONICS FOR EACH PERFORMED ACTIVITY AND THE RECORDED ECG

Activity	Harmonics (Hz)				ECG
	Low Components (0.1-0.8 Hz)		High Components (0.8-3 Hz)		
	Sub-Harmonics	1st	2nd	3rd	
Resting	0.12-0.13	-	-	-	1.46
Jogging	0.14	-	0.9	1.8	1.71
Rowing	0.17	0.71	1.43	2.18	-
Cycling	0.16	-	0.9	1.81	-

Comparison of the various radio channels considered (which not only include radio propagation characteristics, but also embed biomechanical information, such as human motion) for the three activities showed noticeable differences in channel parameters.

The statistical models for each activity show that dynamic radio channels are best described by Rayleigh, Nakagami and Weibull distributions, rather than lognormal distributions. The Rayleigh distribution was consistently the best model for all links and activities, under the test conditions described. Further work is required to determine if this remains true when test conditions differ (e.g., test subject, activity, speed of motion, test environment). In particular, the effect of the environment (off-body scatterers and multipath) on the "best-fit" statistical distribution is expected to be significant.

Moreover, the analysis of the spectrum plots, for the waist-to-chest channel, identified distinct frequency components for each recorded exercise. These components were analyzed in the context of the activities and physiological signals from the breathing process are observed. Thus, the on-body radio channel provides a model for activity classification and potential physiological feature extraction. The work proposed in this paper may open up a new possibility of non-invasive physiological monitoring based on EM sensing from on-body wireless sensor nodes. One potentially interesting avenue for future research is applying this technique to activities with more complex movements (e.g., hurdling, climbing stairs). The use of antennas that radiate along the body surface, or operation at higher frequencies, may allow greater sensitivity to the thoracic motion related to respiration and cardiac activity. Finally, the use of time-frequency analysis, to track how the harmonics change over time, is of some interest.

REFERENCES

[1] P. S. Hall and Y. Hao, *Antennas and propagation for body-centric wireless communications*: Artech House, 2006, ISBN: 9781580534932.

[2] Y. Hao and R. Foster, "Wireless body sensor networks for health-monitoring applications," *Physiological Measurement,* vol. 29, p. R27, 2008.

[3] M. Gallo, P. S. Hall, and M. Bozzetti, "Simulation And Measurement Of Body Dymamics For On-Body Channel Characteirisation," in *IET Seminar on Antennas and Propagation for Body-Centric Wireless Communications, 2007* 2007, pp. 71-74.

[4] Z. H. Hu, M. Gallo, Q. Bai, Y. I. Nechayev, P. S. Hall, and M. Bozzettit, "Measurements and Simulations for On-Body Antenna Design and Propagation Studies," in *The Second European Conference on Antennas and Propagation, EuCAP 2007*, 2007, pp. 1-7.

[5] O. Aziz, B. Lo, R. King, A. Darzi, and Y. Guang-Zhong, "Pervasive body sensor network: an approach to monitoring the post-operative surgical patient," in *International Workshop on Wearable and Implantable Body Sensor Networks, BSN 2006.*, 2006, pp. 4 pp.-18.

[6] L. Atallah, B. Lo, R. King, and Y. Guang-Zhong, "Sensor Placement for Activity Detection Using Wearable Accelerometers," in *International Conference on Body Sensor Networks (BSN), 2010*, 2010, pp. 24-29.

[7] P. Frehill, D. Chambers, and C. Rotariu, "Using Zigbee to Integrate Medical Devices," in *Engineering in Medicine and Biology Society, 2007. EMBS 2007. 29th Annual International Conference of the IEEE*, 2007, pp. 6717-6720.

[8] C. Shih-Lun, L. Ho-Yin, C. Chiung-An, H. Hong-Yi, and L. Ching-Hsing, "Wireless Body Sensor Network With Adaptive Low-Power Design for Biometrics and Healthcare Applications," *Systems Journal, IEEE,* vol. 3, pp. 398-409, 2009.

[9] J. C. Lin, "Noninvasive microwave measurement of respiration," *Proceedings of the IEEE,* vol. 63, pp. 1530-1530, 1975.

[10] J. C. Lin, "Microwave sensing of physiological movement and volume change: a review," *Bioelectromagnetics,* vol. 13, pp. 557-65, 1992.

[11] J. C. Lin, J. Kiernicki, M. Kiernicki, and P. B. Wollschlaeger, "Microwave Apexcardiography," *Microwave Theory and Techniques, IEEE Transactions on,* vol. 27, pp. 618-620, 1979.

[12] A. Pantelopoulos and N. G. Bourbakis, "A Survey on Wearable Sensor-Based Systems for Health Monitoring and Prognosis," *Systems, Man, and Cybernetics, Part C: Applications and Reviews, IEEE Transactions on,* vol. 40, pp. 1-12, 2010.

[13] L. Changzhi, X. Yanming, and J. Lin, "Experiment and Spectral Analysis of a Low-Power Ka-Band Heartbeat Detector Measuring From Four Sides of a Human Body," *Microwave Theory and Techniques, IEEE Transactions on,* vol. 54, pp. 4464-4471, 2006.

[14] A. D. Droitcour, O. Boric-Lubecke, V. M. Lubecke, J. Lin, and G. T. A. Kovacs, "Range correlation and I/Q performance benefits in single-chip silicon Doppler radars for noncontact cardiopulmonary monitoring," *Microwave Theory and Techniques, IEEE Transactions on,* vol. 52, pp. 838-848, 2004.

[15] K. Sang-Gyu, Y. Gi-Ho, and Y. Jong-Gwan, "Wireless RF Vital Signal Sensor Using Autoregressive Spectral Estimation Method," *Antennas and Wireless Propagation Letters, IEEE,* vol. 11, pp. 535-538, 2012.

[16] N. Sazonova, R. C. Browning, and E. Sazonov, "Accurate Prediction of Energy Expenditure Using a Shoe-Based Activity Monitor," *Med Sci Sports Exerc,* Dec 1 2010.

[17] A. R. Guraliuc, P. Barsocchi, Potorti, x, F., and P. Nepa, "Limb Movements Classification Using Wearable Wireless Transceivers," *IEEE Transactions on Information Technology in Biomedicine,* vol. 15, pp. 474-480, 2011.

[18] A. R. Guraliuc, A. A. Serra, P. Nepa, G. Manara, and F. Potorti, "Detection and classification of human arm movements for physical rehabilitation," in *IEEE Antennas and Propagation Society International Symposium (APSURSI), 2010* 2010, pp. 1-4.

[19] G. A. Conway and W. G. Scanlon, "Antennas for Over-Body-Surface Communication at 2.45 GHz," *IEEE Transactions on Antennas and Propagation,* vol. 57, pp. 844-855, 2009.

[20] A. Lea, H. Ping, J. Ollikainen, and R. G. Vaughan, "Propagation Between On-Body Antennas," *IEEE Transactions on Antennas and Propagation,* vol. 57, pp. 3619-3627, 2009.

[21] P. S. Hall, M. Ricci, and T. M. Hee, "Measurements of on-body propagation characteristics," in *Antennas and Propagation Society International Symposium, 2002. IEEE*, 2002, pp. 310-313 vol.2.

[22] S. L. Cotton, W. G. Scanlon, and J. Guy, "The kappa-mu Distribution Applied to the Analysis of Fading in Body to Body Communication

Channels for Fire and Rescue Personnel," *IEEE Antennas and Wireless Propagation Letters,* vol. 7, pp. 66-69, 2008.

[23] L. Akhoondzadeh-asl, P. S. Hall, Y. Nechayev, and I. Khan, "Depolarization in On-Body Communication Channels at 2.45 GHz," *Antennas and Propagation, IEEE Transactions on,* vol. 61, pp. 882-889, 2013.

[24] D. Smith, L. Hanlen, J. Zhang, D. Miniutti, D. Rodda, and B. Gilbert, "First- and second-order statistical characterizations of the dynamic body area propagation channel of various bandwidths," *annals of telecommunications - annales des télécommunications,* vol. 66, pp. 187-203, 2011/04/01 2011.

[25] L. Liu, R. D'Errico, L. Ouvry, P. De Doncker, and C. Oestges, "Dynamic channel modeling at 2.4 GHz for on-body area networks," *Advances in Electronics and Telecommunications-Radio Communication Series: Recent Advances in Wireless Communication Networks,* vol. 2, pp. 18-27, 2011.

[26] K. Minseok, K. Wangchuk, and J. Takada, "Link correlation property in WBAN at 2.4 GHz by multi-link channel measurement," in *Antennas and Propagation (EUCAP), 2012 6th European Conference on*, 2012, pp. 548-552.

[27] L. Lingfeng, S. Van Roy, F. Quitin, P. De Doncker, and C. Oestges, "Statistical characterization and modeling of Doppler spectrum in dynamic on-body channels," *Antennas and Wireless Propagation Letters, IEEE,* vol. 12, pp. 186-189, 2013.

[28] R. D'Errico and L. Ouvry, "Doppler characteristics and correlation proprieties of on-body channels," in *Antennas and Propagation (EUCAP), Proceedings of the 5th European Conference on*, 2011, pp. 2977-2981.

[29] F. Ruijun, Y. Yunxing, Y. Ning, and K. Pahlavan, "Doppler spread analysis of human motions for Body Area Network applications," in *Personal Indoor and Mobile Radio Communications (PIMRC), 2011 IEEE 22nd International Symposium on*, 2011, pp. 2209-2213.

[30] Texas Instruments. (2007). *2.4 GHz IEEE 802.15.4 / ZigBee-ready RF Transceiver*. Available: http://focus.ti.com/lit/ds/symlink/cc2420.pdf

[31] Microchip. (2008). *PIC18F2620 28-Pin Enhanced Flash Microcontrollers with 10-Bit A/D and NanoWatt Technology*. Available: http://ww1.microchip.com/downloads/en/DeviceDoc/39626e.pdf

[32] "IEEE Standard for Local and metropolitan area networks--Part 15.4: Low-Rate Wireless Personal Area Networks (LR-WPANs)," *IEEE Std 802.15.4-2011 (Revision of IEEE Std 802.15.4-2006),* pp. 1-314, 2011.

[33] Microwave Studio, "CST-Computer Simulation Technology," ed, 2013. Available: www.cst.com

[34] M. O. Munoz, R. Foster, and H. Yang, "On-Body Channel Measurement Using Wireless Sensors," *Antennas and Propagation, IEEE Transactions on,* vol. 60, pp. 3397-3406, 2012.

[35] S. L. Cotton and W. G. Scanlon, "Statistical characterisation for a mobile bodyworn personal area network in an indoor multipath environment at 868 MHz," in *Antennas and Propagation, 2006. EuCAP 2006. First European Conference on*, 2006, pp. 1-7.

[36] Y. I. Nechayev, Z. H. Hu, and P. S. Hall, "Short-term and long-term fading of on-body transmission channels at 2.45 GHz," in *Antennas & Propagation Conference, 2009. LAPC 2009. Loughborough*, 2009, pp. 657-660.

[37] L. Birgé and Y. Rozenholc, "How many bins should be put in a regular histogram," *ESAIM: Probability and Statistics,* vol. 10, pp. 24-45, 2006.

[38] D. Freedman and P. Diaconis, "On the histogram as a density estimator: L 2 theory," *Probability theory and related fields,* vol. 57, pp. 453-476, 1981.

[39] P. J. Maud and C. Foster, *Physiological assessment of human fitness*: Human Kinetics Publishers, 2006, ISBN: 073604633X.

[40] CORTEX Medical - Sports - Fitness. (2012). *CORTEX centrepiece: MetaSoft® Studio*. Available: http://www.cortex-medical.de/software_mss_sp_en.htm

[41] P. D. Welch, "The use of fast Fourier transform for the estimation of power spectra: A method based on time averaging over short, modified periodograms," *Audio and Electroacoustics, IEEE Transactions on,* vol. 15, pp. 70-73, 1967.

[42] R. B. Blackman and J. W. Tukey, *"Particular Pairs of Windows", in The measurement of power spectra, from the point of view of communications engineering*: Dover Publications, 1958.

Max O. Munoz received a first class M.Eng. degree in Electronic Engineering from Queen Mary, University of London (QMUL), London, UK., in 2008. The same year, he joined QMUL's Antennas and Electromagnetics Research Group and obtained the Ph.D. degree in 2013.

Currently, he is a Post-doctoral Research Assistant in Queen Mary, University of London and is actively exploring innovative solutions for future wearable technologies. His main research activities include small and compact antennas for low-power wireless sensors operating at microwaves and submillimeter frequencies, flexible and conformal body-worn antennas for medical applications, non-invasive physiological sensing techniques, modelling for body-centric sensor networks, antenna interactions with the human body, indoor radio propagation, active and passive indoor RF localization, design and development of low-power circuits, and RF instrumentation. He has co-authored a book chapter of Autonomous Sensor Networks Collective Sensing Strategies for Analytical Purposes (Springer Series on Chemical Sensors and Biosensors), published a number of journal papers and presented papers in a number of established international conferences, including EuCAP, APS, BSN, MobiHealth and LAPC.

Robert Foster (M-08) received a first class M.Eng. degree in electronics and communications and the Ph.D. degree from the University of Birmingham, Birmingham, U.K., in 2004 and 2008, respectively.

Currently, he is the QUEST Research Programme Manager and Postdoctoral Researcher at Queen Mary College, University of London, London, U.K. He has authored or co-authored a number of conference and journal papers, including contributions in Proceedings of the IEEE and IEEE Transactions on Antennas and Propagation. His current research interests include body-centric wireless communications, wireless sensors, low-power systems, UWB systems, millimeter-wave systems, RF-based positioning systems, and RFID.

Dr. Foster is a member of the Institution of Engineering and Technology (IET), U.K. He is also a member of the IEEE Antennas and Propagation Society, the IEEE Microwave Theory and Techniques Society, and the IEEE Communications Society. He has presented his research at a number of established international conferences, with invited talks at a number of events, including LAPC 2011 and the IET Seminar on Wireless Communication in Buildings, 2011.

Yang Hao (M'00–SM'06 - F'10) received the Ph.D. degree from the Centre for Communications Research (CCR) at the University of Bristol, Bristol, U.K., in 1998. He is currently a professor of antennas and electromagnetics in the Antenna Engineering Group, Queen Mary College, University of London. He is active in a number of areas, including computational electromagnetics, electromagnetic band-gap structures and microwave metamaterials, antennas and radio propagation for body centric wireless networks, active antennas for millimeter/sub-millimeter applications and photonic integrated antennas. He is a co-editor and co-author of the books Antennas and Radio Propagation for Body-Centric Wireless Communications (Boston, MA: Artech House, 2006), and FDTD modelling of Metamaterials: Theory and Applications (Boston, MA: Artech House, 2008), respectively.

Professor Hao is an Associate Editor for the IEEE Antennas and Wireless Propagation Letters, IEEE Transactions on Antennas and Propagation, International Journal of Antennas and Propagation and a honorary editor for the Chinese Journal of Radio Science. He was also a Co-Guest Editor for the IEEE TRANSACTIONS ON ANTENNAS AND PROPAGATION. He is a vice chairman of the Executive Team of IET Antennas and Propagation Professional Network and a member of the New Emerging Technology Committee of the IEEE Antenna and Propagation Society. He is also a member of Board of the European School of Antenna Excellence, a member of EU ASSIST Cost Action and the Virtual Institute for Artificial Electromagnetic Materials and Metamaterials, Metamorphose VI AISBL. He has served as an invited (ISAP07, LAPC07, IWAT08) and keynote speaker (ANTEM05, IWAT'10), a conference General Chair (LAPC08, Metamaterials09), a Session Chair and short course organizer at many international conferences. Professor Hao was elected as a Fellow of the ERA Foundation in 2007 and a Fellow of the IET in 2010.